Crystallographically Aligned Carbon Nanotubes Grown on Few-Layer Graphene Films

D. Patrick Hunley,[†] Stephen L. Johnson,[†] Joseph K. Stieha,[†] Abhishek Sundararajan,[†] Aaron T. Meacham,[†] Ilia N. Ivanov,[‡] and Douglas R. Strachan[†,*]

[†]Department of Physics & Astronomy, University of Kentucky, Lexington, Kentucky 40506, United States, and [‡]Center for Nanophase Materials Sciences, Oak Ridge National Laboratory, Oak Ridge, Tennessee 37831, United States

ABSTRACT Carbon nanotubes are grown on few-layer graphene films using chemical vapor deposition without a carbon feedstock gas. We find that the nanotubes show a striking alignment to specific crystal orientations of the few-layer graphene films. The nanotubes are oriented predominantly at 60 degree intervals and are offset 30 degrees from crystallographically oriented etch tracks, indicating alignment to the armchair axes of the few-layer graphene films. Nanotubes grown on various thicknesses of few-layer graphene under identical process conditions show that the thinnest films, in the sub-6 atomic layer regime, demonstrate significantly improved crystallographic alignment. Intricate crystallographic patterns are also observed having sharp kinks with bending radii less than the ~10 nm lateral resolution of the electron and atomic force microscopy used to image them. Some of these kinks occur independently without interactions between nanotubes while others result when two nanotubes intersect. These intersections can trap nanotubes between two parallel nanotubes resulting in crystallographic back and forth zigzag geometries. These interactions suggest a tip-growth mechanism such that the catalyst particles remain within several nanometers of the few-layer graphene surface as they move leaving a nanotube in their wake.

KEYWORDS: graphene · aligned carbon nanotubes · crystallographic etching · catalysis · chemical vapor deposition

Carbon nanotubes (NTs) and graphene have tremendous potential for future nanoscale applications due to their remarkable physical properties, such as high carrier mobility and mechanical strength.[1,2] To realize the potential of these two closely related materials, both comprising sp^2-bonded honeycomb structured carbon sheets, significant improvements to the crystallographic control over their construction, orientation, and placement at the nanoscale are required.[3] Toward this goal, a number of techniques have been utilized to precisely control the orientation and placement of NTs, such as aligned growth utilizing atomic step-edge templates,[4,5] single-crystal templates,[6−8] flow-alignment,[9,10] electric-field alignment,[11] and combinations of the above techniques yielding novel structures such as serpentines.[12−14] Crystallographic nanoscale control over the construction of graphene and few-layer graphene (FLG) structures has seen progress through nanolithographic methods,[15] crystallographic catalytic etching,[16−18] etch masks made from nanowires and metallic nanojunctions,[19] localized etching with scanning probes,[20,21] ultrasonication,[22,23] and plasma etching of NTs.[24,25] Additional recent efforts in precision nanofabrication have been directed toward the goal of directly growing NTs from carbon sources, such as graphene oxide[26] and reduced graphene oxide,[27] without the need of a feedstock gas. Although NTs have been shown to have a chirality dependent adhesion to graphene,[28] most previous investigations focused on the interactions between NTs and graphene in its bulk graphite form;[29−39] with some of this work showing that NTs grown through laser ablation can be oriented along specific bulk graphite crystal axes.[36]

Here we report the growth of NTs on FLG films using catalytic chemical vapor deposition (CVD) without a carbon feedstock gas. We find that NTs grow along specific crystallographic orientations of the FLG films. Moreover, this crystallographic alignment becomes significantly more pronounced on thinner films that are less than approximately six atomic layers thick. The orientations of the NTs are 30° offset from crystallographic etch directions occurring in graphene,[16,40,41] indicating that the NTs lie along the armchair directions of the FLG lattice. A striking feature of the NTs on FLG is that they make occasional abrupt 60° or 120° changes in direction along the other armchair orientations. These abrupt changes in crystallographic direction also occur when NTs encounter one another, which is indicative of a tip-growth mechanism along the surface of the FLG.

* Address correspondence to doug.strachan@uky.edu.

Received for review April 29, 2011 and accepted July 6, 2011.

Published online July 12, 2011
10.1021/nn201573m

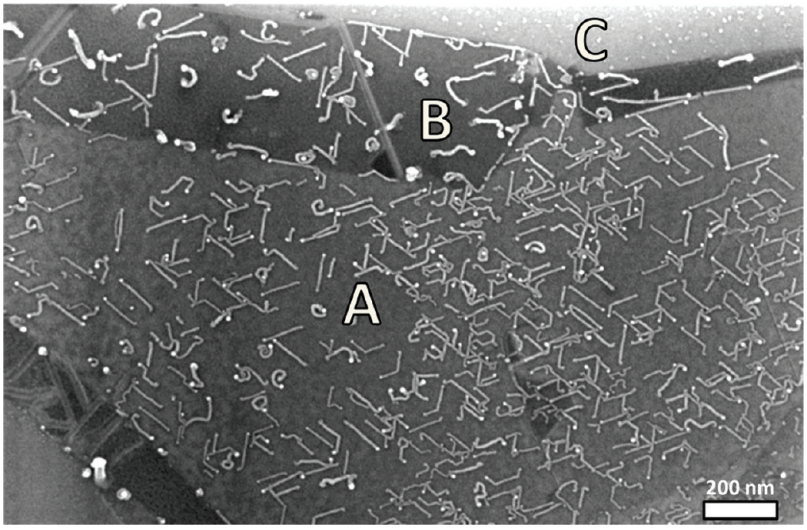

Figure 1. SEM image of NTs aligned to the crystallographic axes of FLG. The region exhibiting the most crystallographic alignment, labeled A in the figure, is ~1.0 nm thick as measured by AFM. The thicker region, labeled B, is ~2.5 nm thick and produced fewer and less aligned NTs than region A. Region C is an exposed portion of the underlying SiO_2 substrate.

RESULTS AND DISCUSSION

Figure 1 shows a scanning electron microscopy (SEM) image of NTs grown on a FLG film ~1.0 nm thick (region "A" in the figure), as measured by atomic force microscopy (AFM). The lines in Figure 1 are NTs which were grown at the elevated temperatures inside the CVD furnace with an Ar and H_2 gas mixture without the need for a carbon feeding gas (see details in Methods section). Unordered NT growth on FLG without feeding gas at elevated temperatures has previously been attributed to residual carbon on the sample surface.[18,42] In contrast to this previous work, our cleaning and catalyst preparation methods promote crystallographically oriented NT growth on FLG samples. Control experiments utilizing an additional methane feedstock gas show inhibited NT growth on the FLG and long NTs only on the exposed SiO_2 substrate. Removal of tape residue using a 400 °C furnace cleaning step prior to catalyst evaporation[43] and using a pristine CVD quartz tube make negligible differences to the amount of NT growth, indicating that the carbon source originates from the FLG and graphite exfoliated onto the wafer. In addition, the NTs in the figure each have a single bright spot at one end, which is likely a catalyst particle. The NT diameters are in the 4 to 10 nm range, as determined by AFM measurements. Also evident in Figure 1 are etch tracks formed through catalytic hydrogenation of the FLG film.[16]

To determine the crystallographic orientation of the NTs, we statistically analyzed their growth on a ~0.4 nm thick FLG flake (Figure 2). This sample contains a significant number of etch tracks and NTs which permit a statistical analysis of their orientations. Figure 2a shows an AFM phase contrast image of the sample, which serves to simultaneously determine the orientation and position of both the NTs and the etch tracks. In this phase image, NTs have a greater contrast on the graphene than the etch tracks, while the etch tracks appear as the longer, fainter lines. Figure 2b shows histograms of the total lengths of all NTs (solid blue line) and etch tracks (dashed red line) in Figure 2a *versus* angle. Each of these histograms show a series of distinct peaks at 60° intervals, with the two sets offset by 30°. Since nickel catalyst particles have long been known to etch graphite predominantly along the zigzag axes,[41] for track widths like those in Figure 2 which are in the majority ~10 nm or greater,[17,40] we deduce that NT formation is mostly occurring along the armchair directions. Future ultrahigh resolution electron microscopy of suspended nanotube on FLG samples would be particularly useful to independently confirm and elucidate their crystallographic characteristics.

The crystallographically aligned growth of NTs on FLG becomes less pronounced as the flake thickness increases. For FLG thicker than about five atomic layers, the crystallographic alignment of CVD-grown NTs is substantially decreased. This thickness-dependent growth is illustrated by the single flake of FLG shown in Figure 3a. This flake contains three regions that have thicknesses of 4.7 (i), 1.8 (ii), and 0.4 nm (iii). Detailed images of the FLG flake and the boundaries of the three regions (i–iii) are shown in the SEM images of Figure 3b–d. The corresponding histograms of length *versus* angle are plotted in Figure 3a. The size of the regions in Figure 3b–d is chosen to include roughly the same amount of total NT length, in order to permit a valid statistical comparison between the three regions. Care was also taken not to select regions where NT growth may have been affected by FLG edges. The histograms in Figure 3a show that under the same growth conditions, the NT alignment along

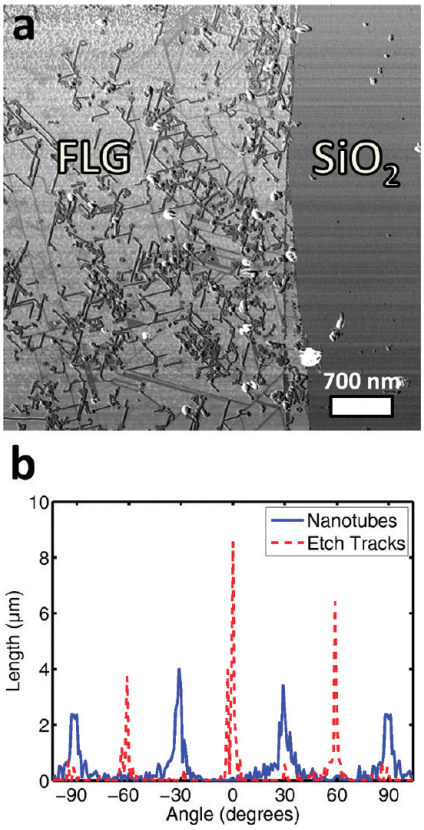

Figure 2. (a) AFM phase image of NTs and etch tracks in graphene. In the image, NTs have a higher contrast on the graphene while the etch tracks are the fainter lines. (b) Histograms generated from the AFM phase image of the total length of all NTs and etch tracks along a given angle, with an angular bin size of 1°. Etch tracks tend to occur every 60°, as represented by the peaks in the histograms, while NT histogram peaks are offset by 30°. Data beyond ±90° are repeated in order to clearly view the peak located at 90°.

the crystallographic axes of the FLG becomes much more pronounced for flakes less than ~6 atomic layers thick. A detailed AFM height analysis of more than 40 NTs in each of the three regions shows only a very slight change in average NT diameter for the various FLG thicknesses (from 6.2 ± 0.7 nm for the thinnest layer to 7.9 ± 1.6 nm for the thickest layer).

In addition to their pronounced crystallographic alignment on thin FLG films, we also find that NTs grown on FLG show abrupt changes in their direction of alignment to the underlying graphene lattice, usually from one armchair direction to another. This change in orientation produces kinks of 60° and 120° in otherwise straight NTs, as seen in Figure 4 panels a and b. Some of these abrupt changes seem to occur independently without interactions between NTs (as pointed to by the red solid arrows in Figure 4 panels a and b), while others result when one NT comes into contact with another (pointed to by the yellow dashed arrow in Figure 4a). The abrupt changes in direction without NT intersections may be due to interactions between the growing NT−catalyst structure and defects or impurities in the FLG or SiO_2 substrate.

The interaction between growing NTs on FLG can also result in intricate patterns. Examples of such patterns are shown in Figure 4c,d, where a growing NT has been bounded by two other NTs to form a crystallographic back-and-forth pattern. This suggests that the NTs grow through a surface-bound, tip-growth mechanism since it would be highly improbable for a fixed catalyst particle to produce such a structure precisely fitting between two other NTs. The formation of such back-and-forth patterns also indicates that the catalyst particles on FLG must remain very close to the surface (within a few nanometers) since NTs less than 10 nm in diameter act as effective barriers to the growth of other NTs.

Such a surface-bound tip-growth mechanism has previously been observed on faceted and atomic steps where nanoparticles slide along the surface leaving a NT behind in its wake.[4,44] Although the intricate patterns we observe support this NT growth process, future *in situ* electron microscopy experiments would be useful to definitively determine the mechanism.

We also observe that NTs do not tend to cross etch tracks. Figure 4e shows a rare occurrence of a NT and etch track intersection, but with the NT having a cut in it. This suggests that the NT was formed first and a nanoparticle cut through it while forming an etch track at a later time. In addition, when a NT reaches a step edge between regions of differing FLG thickness, the nanotube will grow along the edge, as seen in Figure 4f at the intersection between an ~0.5 nm and an ~2.5 nm region.

The typical bending radius we observe at the kinks of the NTs is less than the ~10 nm lateral resolution of the SEM and AFM images. This upper bound to the bending radius is extremely small compared to the micrometer scale bending radii typically observed for NTs when the growth and alignment is understood to involve the lifting up of the catalyst particle from the surface of the substrate.[9,10,12−14] Such a small radius of curvature could indicate that the NTs change crystal direction abruptly rather than bend, which may have potential use in forming NT junctions.[45] Kinked NT growth has been reported along step edges on miscut quartz[5] and along various preferred crystallographic directions on Y-cut and Z-cut quartz substrates due to angular dependent van der Waals interactions.[7,12] NT growth on Z-cut quartz shows similarity to the growth geometries we observe on FLG substrates, with NTs having abrupt changes in direction between the three preferred growth axes which are separated by 60° intervals.

The crystallographic alignment of the NTs along the armchair directions of the FLG could indicate the prevalence of zigzag-oriented NTs. The interaction energy between a carbon nanotube and a graphitic

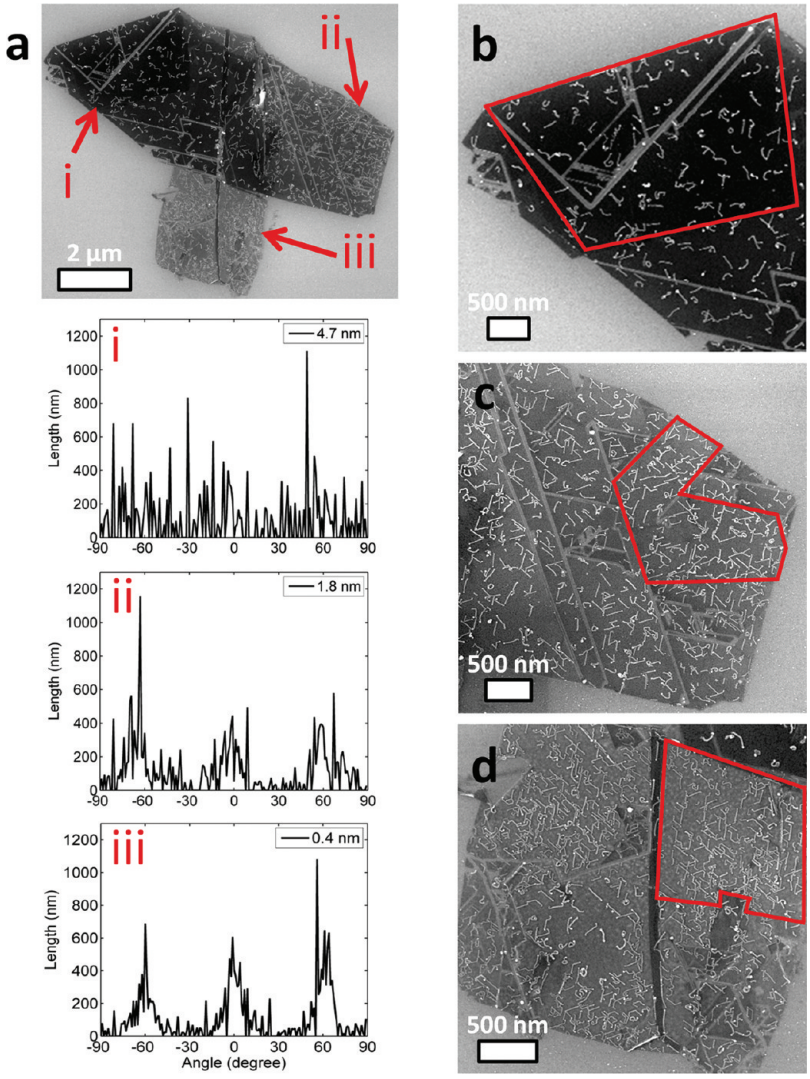

Figure 3. (a) SEM image of NTs grown on regions of a contiguous flake of FLG with thicknesses 4.7 (i), 1.8 (ii), and 0.4 nm (iii). The corresponding histograms generated from the three regions show that crystallographic alignment increases as FLG thickness decreases. (b–d) Higher resolution SEM images showing details of the three locations with the regions used for the histogram analysis outlined in red.

substrate is dependent on the relative orientation of their lattice structures,[28,29,33] with the difference in interaction energy for aligned and misaligned nanotubes being on the order of 10 meV per nanometer of tube length.[35] This interaction energy could play a role during the catalytic formation since the catalyst particle remains within several nanometers of the surface of the FLG sheet. Moreover, since the catalyst particle remains close to the FLG surface during NT growth, the interactions between the catalyst particle and the FLG could also be important in the growth of crystallographically aligned NTs. Recent work has found significant electrostatic screening variations within FLG of various thicknesses,[46] and its interactions with metallic nanoparticles.[47] Such electrostatic interactions may play a role in the variation of crystallographic alignment for various thicknesses of FLG, as found here in Figure 3.

Recent work on single-crystal sapphire has demonstrated that the chirality and diameter of NTs can be influenced by the crystallographic surface of the substrate.[8] Although this supports the possibility that zigzag-oriented NTs may be prevalent on our samples, another recent report on single-crystal quartz has found that chirality and diameter are instead not dependent on the crystalline substrate, even when the NTs are well aligned along specific crystal axes.[7] Thus, future experiments having either atomic resolution or sensitivity to chirality will be required to determine whether the crystal structure of the NTs themselves are influenced by the FLG support.

To utilize the NTs in electronics could require their isolation on insulating substrates away from the FLG support on which they are grown. To demonstrate that these NTs could be transferred to insulating substrates

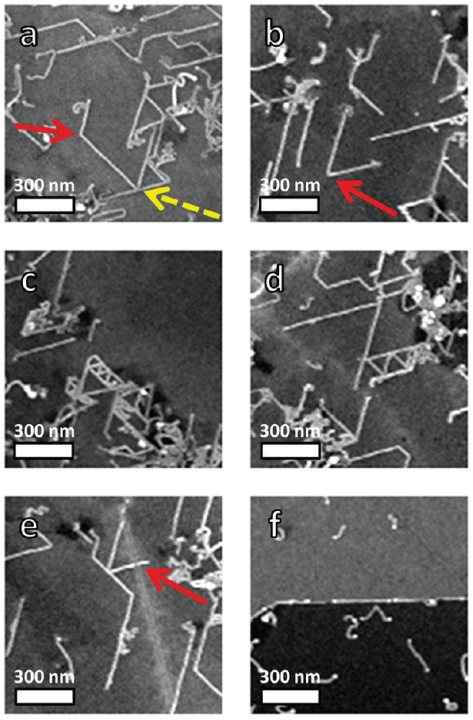

Figure 4. SEM images of NTs showing abrupt changes in crystallographic alignment. (a, b) NTs showing abrupt changes in direction on a FLG film ~0.4 nm thick, as determined by AFM. Red solid arrows point to NTs that abruptly change direction to an alternate crystal axis without interaction with other NTs, while yellow dashed arrow points to a NT that deflects away from another NT. (c, d) A growing NT caught between two parallel NTs can be deflected back and forth to create a zigzag-patterned NT, appearing like a sequence of equilateral triangles. (e) Crystallographically aligned NT that is etched through by a catalyst particle. The location of the etch track through the NT is pointed to by the solid red arrow. (f) NTs grown along a step edge between two FLG regions of ~0.5 and ~2.5 nm thicknesses.

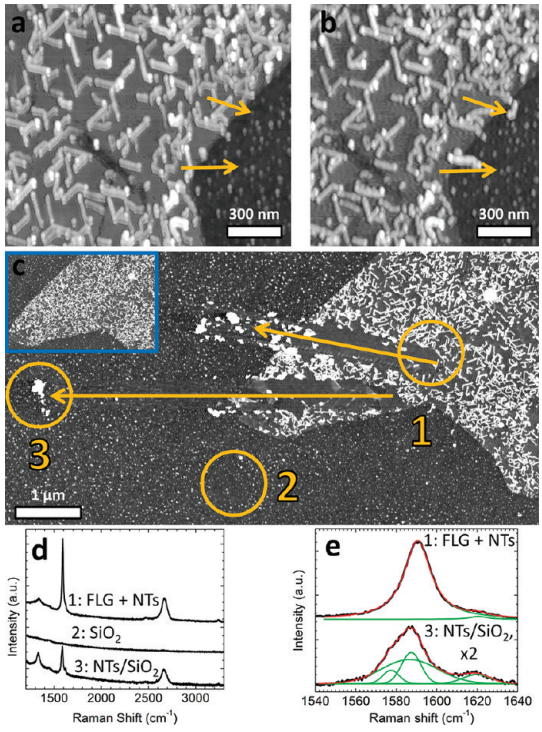

Figure 5. (a) AFM height image of NTs on ~1.1 nm thick FLG before application of the AFM strokes represented by the arrows. (b) AFM image of same region after application of the AFM strokes showing NTs displaced off of the FLG substrate. (c) AFM image of two regions of the same sample where ~10 AFM strokes have moved a large number of NTs through nanomanipulation with an AFM tip in the directions indicated by the arrows. Inset shows an AFM image of the sample before the NTs were moved. (d) Micro-Raman spectra of the three regions circled in panel c. (e) Expanded view of G band peaks comparing detailed signal from the region containing NTs on FLG (region 1) to the region containing the deposited NTs on SiO_2 (region 3). The signal from the isolated NTs in region 3 is multiplied by a factor of 2. Red curves are fits comprising the sum of the Lorentzian line shapes plotted in green.

we have utilized an AFM tip to drag them off of the FLG flakes and onto the nearby SiO_2 substrate. Figure 5 shows the before (a) and after (b) AFM height images of NTs which have been dragged from an ~1.1 nm thick FLG onto the exposed SiO_2 with the AFM strokes represented by the arrows. This physical transfer of the NTs shows that they are not covalently bound to the FLG surface.

Figure 5c shows another region on the same FLG sample where ~10 adjacent strokes of an AFM tip (as indicated by the arrows) have dragged NTs completely off of the FLG and onto the nearby SiO_2 to two separate locations. Figure 5d shows micro-Raman spectra taken at the three circled regions marked in Figure 5c. The Raman measurements taken over the NTs and FLG (region 1) show three distinct peaks in Figure 5d that correspond to the well-known D, G, and G′ bands characteristic of sp^2 bonded carbon allotropes.[48] Raman measurements over the clump of NTs that were dragged from the FLG and displaced over the SiO_2 substrate (region 3) show a similar sp^2 bonded carbon response, whereas a control experiment over the SiO_2 (region 2) shows no appreciable Raman response. These results are an indication that the NTs we observe in fact comprise sp^2 bonded carbon. Moreover, in Figure 5e, a detailed comparison of the G peaks of regions 1 and 3 shows that the shape is significantly more complex for the isolated NTs over the SiO_2. When the NTs are isolated away from the FLG, which contributes a large single-Lorentzian background peak (upper curve), a multi-Lorentzian peak typical of carbon NTs is revealed (lower curve).[48]

CONCLUSIONS

In summary, we report the CVD growth, without a feedstock gas, of NTs that are aligned to the crystal lattice of an underlying FLG support. Due to the presence of simultaneously produced etch tracks in the FLG, we can establish the relative crystallographic orientation of the NTs and we find that the majority of the alignment is along the armchair axes of the FLG,

suggesting the prevalence of zigzag NTs. This crystallographic alignment appears much more pronounced in FLG films thinner than six atomic layers, indicating that electrostatic interactions with the catalyst particles may have a role in the NT growth mechanism. We have also observed NTs with sharp kinks having angles of 60° and 120°. These kinks can occur independently without the NTs interacting with each other. The sharp kinks are also formed at locations where NTs intersect and interact with each other resulting in crystallographic patterns, indicative of a tip-growth mechanism where catalyst particles remain within several nanometers of the FLG surface. These crystallographically oriented geometries could prove useful as kinked NT junction structures for future nanoelectronic applications.[45] To achieve such electronic applications, it would be useful to move the resulting NTs to an insulating substrate. We have demonstrated that NT transfer to an insulating substrate is possible by successfully dragging them with an AFM tip. This dragging technique has been used to isolate a group of NTs away from the FLG support in order to perform Raman spectroscopy, which confirms that the NTs are made of sp^2 bonded carbon. Other more elaborate methods for nanoscale transfer that are currently being developed[49] might be capable of precisely placing the NTs on insulating substrates without disturbing their as-grown geometrical arrangements.

METHODS

Crystallographically aligned NTs on FLG samples were prepared on p^+-doped silicon substrates having a 300 nm thermal oxide layer. The substrates were ultrasonicated in acetone, isopropyl alcohol, and deionized water for 3 min each using a Branson 2510 Bransonic Ultrasonic Cleaner. The substrates were then subjected to UV ozone (UVO) cleaning for 15 min in a NovaScan PSD Series Digital UV Ozone System. Highly ordered pyrolytic graphite (HOPG) was then mechanically exfoliated onto the substrates.[50] Catalyst material was deposited onto the substrate using electron-beam evaporation of a nominally 0.2 Å thick film of Ni to form catalyst particles. Samples were then placed in a chemical vapor deposition (CVD) furnace (Thermo Scientific Lindberg, model TF55035C) with a gas flow of 850 and 150 sccm of Ar and H_2 (determined with MKS Mass-Flo controllers with MKS type 247D four-channel readout), respectively, where they were annealed at 500 °C for 30–60 min and then immediately heated to 900 °C for 60 min in order to grow the NTs. Temperatures were achieved in both steps using a controlled ramp rate of 50 °C per min. Immediately following the growth period, the samples were allowed to cool to room temperature.

Control experiments were performed in the slightly modified (from above) gas flows of 700 sccm Ar and 150 sccm H_2 in order to determine the effects of a 2500 sccm CH_4 feedstock gas. Two sets of control samples were prepared; with and without an additional tape residue removing step performed prior to Ni evaporation. The tape residue removal was performed in the CVD system at 400 °C for 1 h with a gas mixture of 340 sccm Ar and 380 sccm of H2.

AFM height measurement, imaging, and nanomanipulation were performed with an Asylum Research MFP-3D AFM. AFM height measurement and imaging were performed in intermittent contact mode. Nanomanipulation of NTs was performed in contact mode using the Asylum Research MicroAngelo nanolithography and nanomanipulation package. SEM imaging was performed with a Zeiss Supra 35 field-emission SEM with a Gemini Column. Raman spectroscopy measurements were performed with a Renishaw 100 confocal micro-Raman system with a CCD detector; 633 nm excitation of a HeNe laser was focused to ~1 μm spot size with a 100× objective. Spectra were acquired using a 60 s integration time.

Histogram analysis was performed by first digitizing the locations of NTs and/or etch tracks with the use of a MatLab code we developed. This code allows us to trace over a digital image of NTs and etch tracks with a series of short straight lines down to approximately 1 nm in length. The code stores the length, direction, and position of each NT and etch track within an analyzed region. Histograms, as in Figure 2b, are generated by summing the total length for all the lines that fall within a specific angular bin.

Acknowledgment. The authors acknowledge the support from the National Science Foundation (NSF) through Grant DMR-0805136, the Kentucky NSF EPSCoR program through award EPS-0814194, and the University of Kentucky (UK) Center for Advanced Materials (CAM). A portion of this research was conducted at the Center for Nanophase Materials Sciences, which is sponsored at Oak Ridge National Laboratory by the Office of Basic Energy Sciences, U.S. Department of Energy.

REFERENCES AND NOTES

1. Saito, R.; Dresselhaus, G.; Dresselhaus, M. S. *Physical Properties of Carbon Nanotubes*; Imperial College Press: London, 1998.
2. Geim, A. K.; Novoselov, K. S. The Rise of Graphene. *Nat. Mater.* **2007**, *6*, 183–191.
3. Zhou, W. W.; Ding, L.; Liu, J. Role of Catalysts in the Surface Synthesis of Single-Walled Carbon Nanotubes. *Nano Res.* **2009**, *2*, 593–598.
4. Ismach, A.; Segev, L.; Wachtel, E.; Joselevich, E. Atomic-Step-Templated Formation of Single Wall Carbon Nanotube Patterns. *Angew. Chem., Int. Ed.* **2004**, *43*, 6140–6143.
5. Kocabas, C.; Hur, S.-H.; Gaur, A.; Meitl, M. A.; Shim, M.; Rogers, J. A. Guided Growth of Large-Scale, Horizontally Aligned Arrays of Single-Walled Carbon Nanotubes and Their Use in Thin-Film Transistors. *Small* **2005**, *1*, 1110–1116.
6. Han, S.; Liu, X.; Zhou, C. Template-Free Directional Growth of Single-Walled Carbon Nanotubes on a- and R-Plane Sapphire. *J. Am. Chem. Soc.* **2005**, *127*, 5294–5295.
7. Xiao, J.; Dunham, S.; Liu, P.; Zhang, Y.; Kocabas, C.; Moh, L.; Huang, Y.; Hwang, K.-C.; Lu, C.; Huang, W.; Rogers, J. A. Alignment Controlled Growth of Single-Walled Carbon Nanotubes on Quartz Substrates. *Nano Lett.* **2009**, *9*, 4311–4319.
8. Ishigami, N.; Ago, H.; Imamoto, K.; Tsuji, M.; Iakoubovskii, K.; Minami, N. Crystal Plane Dependent Growth of Aligned Single-Walled Carbon Nanotubes on Sapphire. *J. Am. Chem. Soc.* **2008**, *130*, 9918–9924.
9. Huang, S.; Cai, X.; Liu, J. Growth of Millimeter-Long and Horizontally Aligned Single-Walled Carbon Nanotubes on Flat Substrates. *J. Am. Chem. Soc.* **2003**, *125*, 5636–5637.
10. Huang, S. M.; Woodson, M.; Smalley, R.; Liu, J. Growth Mechanism of Oriented Long Single Walled Carbon Nanotubes Using "Fast-Heating" Chemical Vapor Deposition Process. *Nano Lett.* **2004**, *4*, 1025–1028.
11. Zhang, Y.; Chang, A.; Cao, J.; Wang, Q.; Kim, W.; Li, Y.; Morris, N.; Yenilmez, E.; Kong, J.; Dai, H. Electric-Field-Directed Growth of Aligned Single-Walled Carbon Nanotubes. *Appl. Phys. Lett.* **2001**, *79*, 3155–3157.
12. Kocabas, C.; Kang, S. J.; Ozel, T.; Shim, M.; Rogers, J. A. Improved Synthesis of Aligned Arrays of Single-Walled

Carbon Nanotubes and Their Implementation in Thin Film Type Transistors. *J. Phys. Chem. C* **2007**, *111*, 17879–17886.
13. Jeon, S.; Lee, C.; Tang, J. Y.; Hone, J.; Nuckolls, C. Growth of Serpentine Carbon Nanotubes on Quartz Substrates and Their Electrical Properties. *Nano Research* **2008**, *1*, 427–433.
14. Geblinger, N.; Ismach, A.; Joselevich, E. Self-Organized Nanotube Serpentines. *Nat. Nanotechnol.* **2008**, *3*, 195–200.
15. Han, M. Y.; Ozyilmaz, B.; Zhang, Y.; Kim, P. Energy Band-Gap Engineering of Graphene Nanoribbons *Phys. Rev. Lett.* **2007**, 98, Art. No. 206805.
16. Datta, S. S.; Strachan, D. R.; Khamis, S. M.; Johnson, A. T. Crystallographic Etching of Few-Layer Graphene. *Nano Lett.* **2008**, *8*, 1912–1915.
17. Ci, L.; Xu, Z. P.; Wang, L. L.; Gao, W.; Ding, F.; Kelly, K. F.; Yakobson, B. I.; Ajayan, P. M. Controlled Nanocutting of Graphene. *Nano Res.* **2008**, *1*, 116–122.
18. Campos, L. C.; Manfrinato, V. R.; Sanchez-Yamagishi, J. D.; Kong, J.; Jarillo-Herrero, P. Anisotropic Etching and Nanoribbon Formation in Single-Layer Graphene. *Nano Lett.* **2009**, *9*, 2600–2604.
19. Lu, Y.; Goldsmith, B.; Strachan, D. R.; Lim, J. H.; Luo, Z.; Johnson, A. T. C. High-On/Off-Ratio Graphene Nanoconstriction Field-Effect Transistor. *Small* **2010**, *6*, 2748–2754.
20. Tapaszto, L.; Dobrik, G.; Lambin, P.; Biro, L. P. Tailoring the Atomic Structure of Graphene Nanoribbons by Scanning Tunnelling Microscope Lithography. *Nat. Nanotechnol.* **2008**, *3*, 397–401.
21. He, Y. D.; Dong, H. L.; Li, T.; Wang, C. L.; Shao, W.; Zhang, Y. J.; Jiang, L.; Hu, W. P. Graphene and Graphene Oxide Nanogap Electrodes Fabricated by Atomic Force Microscopy Nanolithography *Appl. Phys. Lett.*, *97*, 3.
22. Jiao, L. Y.; Wang, X. R.; Diankov, G.; Wang, H. L.; Dai, H. J. Facile Synthesis of High-Quality Graphene Nanoribbons. *Nat. Nanotechnol.* **2010**, *5*, 321–325.
23. Li, X.; Wang, X.; Zhang, L.; Lee, S.; Dai, H. Chemically Derived, Ultrasmooth Graphene Nanoribbon Semiconductors. *Science* **2008**, *319*, 1229–1232.
24. Jiao, L.; Zhang, L.; Wang, X.; Diankov, G.; Dai, H. Narrow Graphene Nanoribbons from Carbon Nanotubes. *Nature* **2009**, *458*, 877–880.
25. Kosynkin, D. V.; Higginbotham, A. L.; Sinitskii, A.; Lomeda, J. R.; Dimiev, A.; Price, B. K.; Tour, J. M. Longitudinal Unzipping of Carbon Nanotubes to Form Graphene Nanoribbons. *Nature* **2009**, *458*, 872–876.
26. Cao, X. H.; He, Q. Y.; Shi, W. H.; Li, B.; Zeng, Z. Y.; Shi, Y. M.; Yan, Q. Y.; Zhang, H. Graphene Oxide as a Carbon Source for Controlled Growth of Carbon Nanowires. *Small* **2011**, *7*, 1199–1202.
27. Li, B.; Cao, X. H.; Ong, H. G.; Cheah, J. W.; Zhou, X. Z.; Yin, Z. Y.; Li, H.; Wang, J. L.; Boey, F.; Huang, W.; Zhang, H. All-Carbon Electronic Devices Fabricated by Directly Grown Single-Walled Carbon Nanotubes on Reduced Graphene Oxide Electrodes. *Adv. Mater.* **2010**, *22*, 3058–3061.
28. Ortolani, L.; Houdellier, F.; Monthioux, M.; Morandi, V. Chirality Dependent Surface Adhesion of Single-Walled Carbon Nanotubes on Graphene Surfaces *Carbon*, *48*, 3050-3056.
29. Falvo, M. R.; Taylor, R. M.; Helser, A.; Chi, V.; Brooks, F. P.; Washburn, S.; Superfine, R. Nanometre-Scale Rolling and Sliding of Carbon Nanotubes. *Nature* **1999**, *397*, 236–238.
30. Paulson, S.; Helser, A.; Nardelli, M. B.; Taylor, R. M.; Falvo, M.; Superfine, R.; Washburn, S. Tunable Resistance of a Carbon Nanotube-Graphite Interface. *Science* **2000**, *290*, 1742–1744.
31. Liu, J.; Rinzler, A. G.; Dai, H. J.; Hafner, J. H.; Bradley, R. K.; Boul, P. J.; Lu, A.; Iverson, T.; Shelimov, K.; Huffman, C. B.; *; et al*. Fullerene Pipes. *Science* **1998**, *280*, 1253–1256.
32. Falvo, M. R.; Steele, J.; Taylor, R. M.; Superfine, R. Gearlike Rolling Motion Mediated by Commensurate Contact: Carbon Nanotubes on HOPG. *Phys. Rev. B* **2000**, *62*, 10665–10667.
33. Buldum, A.; Lu, J. P. Atomic Scale Sliding and Rolling of Carbon Nanotubes. *Phys. Rev. Lett.* **1999**, *83*, 5050–5053.
34. Yanagi, H.; Sawada, E.; Manivannan, A.; Nagahara, L. A. Self-Orientation of Short Single-Walled Carbon Nanotubes Deposited on Graphite. *Appl. Phys. Lett.* **2001**, *78*, 1355–1357.
35. Rettig, C.; Bodecker, M.; Hovel, H. Carbon-Nanotubes on Graphite: Alignment of Lattice Structure. *J. Phys. D, Appl. Phys.* **2003**, *36*, 818–822.
36. Yi, J. H.; El Khakani, M. A. Highly Oriented Planar Arrays of SWCNTs Grown onto HOPG Substrates by Means of an 'All-Laser' Process. *Chem. Phys. Lett.* **2005**, *413*, 182–187.
37. Miura, K.; Takagi, T.; Kamiya, S.; Sahashi, T.; Yamauchi, M. Natural Rolling of Zigzag Multiwalled Carbon Nanotubes on Graphite. *Nano Lett.* **2001**, *1*, 161–163.
38. Hovel, H.; Bodecker, M.; Grimm, B.; Rettig, C. Growth Mechanisms of Carbon Nanotubes Using Controlled Production in Ultrahigh Vacuum. *J. Appl. Phys.* **2002**, *92*, 771–777.
39. Kuo, W. S.; Ko, T. H.; Lu, H. F. Growing Carbon Nanotubes on Graphite Nanosheets. *Micro Nano Lett.* **2009**, *4*, 128–132.
40. Schaffel, F.; Wilson, M.; Bachmatiuk, A.; Rummeli, M. H.; Queitsch, U.; Rellinghaus, B.; Briggs, G. A. D.; Warner, J. H. Atomic Resolution Imaging of the Edges of Catalytically Etched Suspended Few-Layer Graphene. *ACS Nano* **2011**, *5*, 1975–1983.
41. Tomita, A.; Tamai, Y. Optical Microscopic Study on Catalytic-Hydrogenation of Graphite. *J. Phys. Chem.* **1974**, *78*, 2254–2258.
42. Schaffel, F.; Warner, J. H.; Bachmatiuk, A.; Rellinghaus, B.; Buchner, B.; Schultz, L.; Rummeli, M. H. Shedding Light on the Crystallographic Etching of Multilayer Graphene at the Atomic Scale. *Nano Res.* **2009**, *2*, 695–705.
43. Ishigami, M.; Chen, J. H.; Cullen, W. G.; Fuhrer, M. S.; Williams, E. D. Atomic Structure of Graphene on SiO_2. *Nano Lett.* **2007**, *7*, 1643–1648.
44. Ismach, A.; Kantorovich, D.; Joselevich, E. Carbon Nanotube Graphoepitaxy: Highly Oriented Growth by Faceted Nanosteps. *J. Am. Chem. Soc.* **2005**, *127*, 11554–11555.
45. Yao, Z.; Postma, H. W. C.; Balents, L.; Dekker, C. Carbon Nanotube Intramolecular Junctions. *Nature* **1999**, *402*, 273–276.
46. Datta, S. S.; Strachan, D. R.; Mele, E. J.; Johnson, A. T. Surface Potentials and Layer Charge Distributions in Few-Layer Graphene Films. *Nano Lett.* **2009**, *9*, 7–11.
47. Luo, Z.; Somers, L. A.; Dan, Y.; Ly, T.; Kybert, N. J.; Mele, E. J.; Johnson, A. T. C. Size-Selective Nanoparticle Growth on Few-Layer Graphene Films *Nano Lett.*, *10*, 777-781.
48. Dresselhaus, M. S.; Jorio, A.; Hofmann, M.; Dresselhaus, G.; Saito, R. Perspectives on Carbon Nanotubes and Graphene Raman Spectroscopy. *Nano Lett.* **2010**, *10*, 751–758.
49. Schneider, G. F.; Calado, V. E.; Zandbergen, H.; Vandersypen, L. M. K.; Dekker, C. Wedging Transfer of Nanostructures. *Nano Lett.* **2010**, *10*, 1912–1916.
50. Novoselov, K. S.; Geim, A. K.; Morozov, S. V.; Jiang, D.; Zhang, Y.; Dubonos, S. V.; Grigorieva, I. V.; Firsov, A. A. Electric Field Effect in Atomically Thin Carbon Films. *Science* **2004**, *306*, 666–669.